# Applications of 21cm Radio Astrophysics

Sanjay A. Raman (Partner: Charles Wang)*
*MIT Department of Physics*
(Dated: February 12, 2022)

Hyperfine transitions between the Hydrogen ground state levels emit radiation at $f_0 = 1420.4$ MHz (around 21cm wavelength). We use the SRT, a radio telescope located on the MIT campus, to measure radiation around 21cm. Using the SRT, we compute the brightness temperature of the sun. We also use measurements of 21cm radiation from various galactic sources to derive the rotation curve of the Milky Way. We find that the rotation curve does not obey the formula predicted by Kepler's laws, confirming the existence of dark matter.

## I. INTRODUCTION: RADIO ASTRONOMY

The history of astronomy is almost as long as the history of human civilization itself: Since ancient times, people have always been observing and recording patterns in the night sky. The modern discipline of astronomy has used advanced telescopes to probe far beyond the ancient peoples' observations of stars. In recent times, *radio astronomy* has attracted much interest. Telescopes operating using the radio frequencies can make out features indiscernible to visible-light telescopes.

### I.1. The 21cm Line

A particularly important radio frequency in astronomy is the Hydrogen 21cm line. The energy levels of the Hydrogen ground state have a small splitting due to the orientation of the electron spin, transitions between which result in the emission of a photon with frequency $f_0 = 1420.4$ MHz (which corresponds to a wavelength around 21cm).

The 21cm line is important to astrophysics, since it allows us to determine the velocity of 21cm-emitting sources via the Doppler shift. More precisely, if a Hydrogen-containing source emits 21cm radiation at frequency $f_0$, the telelescope observes a frequency $f_{\text{obs}}$, where

$$f_{\text{obs}} = f_0\sqrt{\frac{1-v/c}{1+v/c}}. \tag{1}$$

Here $v$ is the component of the relative velocity of the source away from the telescope along the line-of-sight.

### I.2. Experimental Outline and Apparatus

We used 21cm radiation to make two measurements. First, we used radio-frequency data to measure the brightness temperature of the sun around 21cm. Second, we measured the frequency profiles around the 21cm line from various galactic sources in the Milky Way and used this to derive the rotation curve of the galaxy.

To make our measurements of 21cm radiation, we used the Small Radio Telescope (SRT) located on the MIT campus. The SRT is a computer-controlled parabolic antenna with a receiver attuned to frequencies around the 21cm line $f_0 = 1420.4$ MHz. Radio-frequency signals at the receiver are amplified and digitized; using the discrete Fourier transform, the frequency profile of radiation intensity is displayed.

## II. BRIGHTNESS TEMPERATURE OF THE SUN

### II.1. Theory

The brightness temperature of the sun can be calculated using the SRT. When radiation from the sun is received at the antenna, a temperature value $T_{\text{Ant}}$ (proportional to the power received by the antenna) is measured, which is related to the sun's temperature $T_\odot$ by the following formula:

$$T_{\text{Ant}} = \eta T_\odot \frac{\Omega_\odot}{\Omega_{\text{BW}}} \tag{2}$$

Here $0 < \eta < 1$ is the efficiency of the antenna, $\Omega_\odot$ is the solid angle of the sun in the sky, and $\Omega_{\text{BW}}$ is the solid angle of the beam.

We made several temperature measurements at different angular displacements $\theta$ from the sun. From the theory of wave optics, we should expect the antenna temperature at displacement $\theta$ to satisfy the following distribution:

$$T_{\text{Ant}} = T_{\text{bkg}} + T_0\frac{J_1(a\sin\theta)}{a\sin\theta} \tag{3}$$

for some constant $a$, where $J_1(x)$ is a Bessel function of the first kind. Here $T_0$ is the peak antenna temperature and $T_{\text{bkg}}$ is the background antenna temperature in the absence of any sources. The temperature $T_\odot$ of the sun can be calculated by integrating over the full angular distribution and using Eq. 2. The result is

$$T_\odot = \frac{4\pi T_0}{\eta a^2 \Omega_\odot}. \tag{4}$$

* sanjayra@mit.edu; http://web.mit.edu/8.13/

### II.2. Experimental Procedure

#### *II.2.1. Offset Calibration and n-point Scans*

Before we collected the data to determine the brightness temperature of the sun, we calibrated the telescope offset using $n$-point scans. The targeting system of the telescope is not perfectly accurate, and as a result, a source could be located at a small offset from where the telescope is pointed.

To determine this offset, we measured the temperature at 25 points within a $4^\circ \times 4^\circ$ grid centered at the telescope targeting system's determination of the sun's location. From this, we produced a contour plot of the temperature in this range. The brightest spot was then deemed to be the true location of the sun, and from this, the offset was computed.

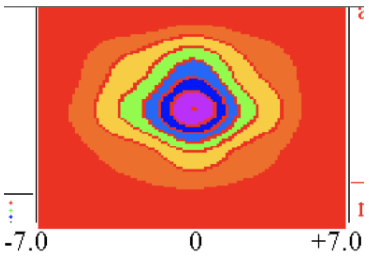


FIG. 1. $n$-point scan of the sun. From this scan, the offset was determined to be $(\text{az}, \text{el}) = (1.^\circ, 2.^\circ)$.

From an analysis of our $n$-point scan, we determined the appropriate offset to be be $(\text{az}, \text{el}) = (1.^\circ, 2.^\circ)$.

#### *II.2.2. Experimental Procedure*

To measure the brightness temperature of the sun, we conducted two independent trials. In each trial, we measured the radiation centered at the frequency $f = 1423.0$ MHz with bandwidth 0.125 MHZ. We then measured the antenna temperature at various azimuthal separations $\theta$ from the sun's position (using the offset determined), where $\theta \in \{-30.^\circ, -29.^\circ, \cdots, 30.^\circ\}$.

### II.3. Data

For each trial, we made a plot of antenna temperature vs. azimuthal offset. As an example, the plot made for trial #1 along with the Bessel function fit as per Eq. 3 is shown in Fig. 2.

### II.4. Analysis and Results

For both trials, we computed the values of $T_0$ and $a$ from the fit; from this, we deduced the brightness temperature $T$ of the sun using Eq. 4. Averaging over both trials, we found

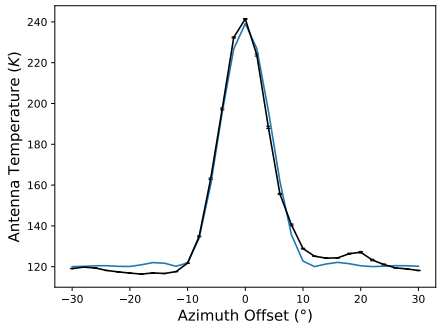


FIG. 2. A plot of the antenna temperature vs. azimuthal offset for trial #1, along with the a least-squares Bessel function fit (see Eq. 3)

$$T_\odot = (5.9 \pm 0.7) \times 10^4 \text{ K}. \tag{5}$$

We estimated the error bar on in $T_\odot$ by considering several different sources of uncertainty:

- The efficiency $\eta$ of the telescope was not known exactly; its value was quoted as $\eta = 0.5 \pm 0.05$.
- We estimated the statistical uncertainty by taking the standard error between our two trials; this yielded around a 4% error bar.
- The calibration constant (used to determine the antenna temperature from the raw counts) was uncertain to about 7%.

Our result for $T_\odot$ agrees with the literature (see for example [1, 2]). In particular, at the time the measurement was made, the sun was near a minimum in the solar cycle [3]; thus, we expect our measurements of the sun's temperature to be lower than some previous measurements.

Note that our result for the brightness temperature of the sun is far greater than the surface temperature of the sun ($\sim 5770$ K). We postualted that the discrepancy arose due an additional contribution to the observed radiation at 21cm from the motion of electrons within the sun's corona.

## III. ROTATION CURVE OF THE MILKY WAY

### III.1. Theory

Another application of 21cm radio astrophysics is to the measurement of rotation curve of the Milky Way galaxy. Here we define the rotation curve to be the tangential velocity $v$ of a source as a function of $r$, its radial distance to the galactic center (Sagittarius A). Using

Kepler's laws, we can derive a theoretical expression for $v(r)$. If $M(r)$ is the mass contained within a sphere of radius $r$ within the galaxy, we have

$$v(r) = \sqrt{\frac{GM(r)}{r}}. \tag{6}$$

Thus, measuring the rotation curve allows us to deduce the density of the galaxy as a function of radius. Now, the vast majority of the stars within the galaxy are contained within the galactic bulge $r \lesssim 1.5$ kpc [4]. As a result, we should expect $M(r)$ to be essentially constant for $r \gtrsim 1.5$ kpc and certainly for $r \gtrsim 4$ kpc. We predict

$$v(r) \propto \frac{1}{\sqrt{r}}, \quad r \gtrsim 4 \text{ kpc}. \tag{7}$$

To measure $v(r)$, we measure the Doppler shift of the Hydrogen 21cm line as discussed in Sec. I.1. Consider now a measurement along the line of galactic longitude $l$ relative to the Local Standard of Rest (LSR). There are several sources contributing 21cm radiation, as shown in Fig. 3.

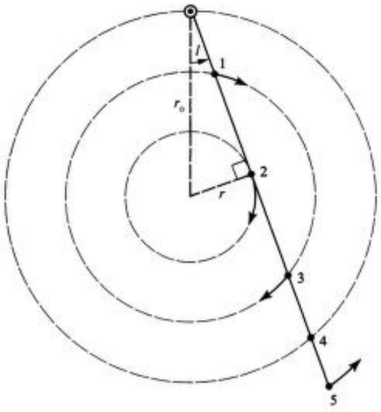


FIG. 3. Different sources of radiation along galactic longitude $l$. Figure from [4].

The source at point 2 in Fig. 3 is moving at the largest parallel relative velocity away from the LSR out of all of the points with galactic longitude $l$. Hence, the frequency $f_{\text{max redshift}}$ with the largest redshift in the frequency profile will correspond precisely to radiation from point 2 in Fig. 3. As shown in [4], we can use $f_{\text{max redshift}}$ to deduce the tangential velocity $v(r)$ at radius $r = r_\odot \sin l$:

$$v(r) = \frac{f_0 - f_{\text{max redshift}}}{f_0} - v_{\text{LSR}} + v_\odot \sin l \tag{8}$$

where $v_{\text{LSR}}$ is the velocity of the telescope relative to the LSR along the line of sight of galactic longitude $l$ and $v_\odot$ is the tangential velocity of the LSR. The value of $v_{\text{LSR}}$ is measured by the SRT, while $v_\odot = 220 \pm 20$ km/$s$ is a well-known tabulated value. Note that Eq. 8 only holds when $r \leq r_\odot$ or $-90° \leq l \leq 90°$, as for $r \geq r_\odot$ we would not be able to draw a tangent line to a circle of radius $r$ as in Fig. 3.

### III.2. Experimental Procedure

To determine the rotation curve, we measured radio frequencies centered at $\sim$ 1420.4 MHz with a bandwidth of 1.2 MHz for each galactic longitude $l \in \{0°, 5°, \cdots, 90°\}$ for 20 minutes each. For the frequency profile at each longitude $l$, we computed $f_{\text{max redshift}}$, and using Eq. 8, we found $v(r_\odot \sin l)$ for each $l$.

### III.3. Data

An example frequency profile collected for galactic longitude $l = 75°$ is shown in Fig. 4. When calculating this frequency profile, we found there to be nonzero background radiation outside the signal region. However, we found by direct observation of the empty sky that the background frequency profile had a linear shape. Thus, we fit a linear function to the extreme lowest and highest frequency "sidebands" and subtracted off the linear fit. The error bars on each frequency bin were determined by taking the RMSE about the linear fit in the sideband regions.

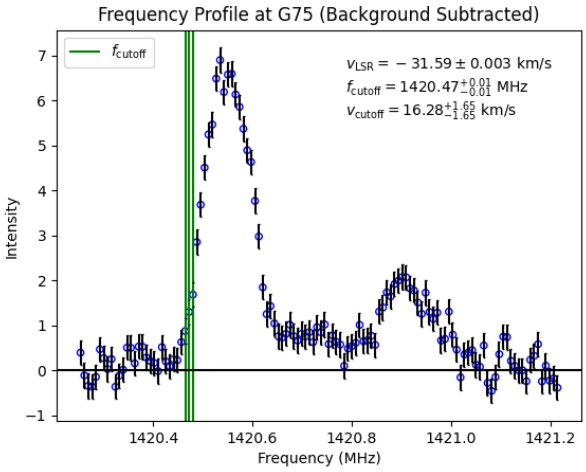


FIG. 4. Intensity vs. Frequency (MHz) observed at G90 after subtracting off the background fit. The vertical green line at $f_{\text{cutoff}} = 1420.47 \pm 0.01$ MHz marks the frequency of maximum redshift appearing at a level $3\sigma$ above the background. Note that units are not provided for the vertical axis, since the exact scaling of the vertical axis is not known. This is, however, irrelevant to the calculation of $f_{\text{cutoff}}$.

We then computed the value of $f_{\text{cutoff}}$, which was the frequency with the largest redshift found at a statistically significant level of $3\sigma$ above the background. As we will show in Sec. III.4.2, the value of $f_{\text{cutoff}}$ is used to calculate $f_{\text{max redshift}}$ and thus $v(r)$.

### III.4. Analysis and Uncertainties

In addition to the usual statistical uncertainty, there were several nontrivial sources of systematic uncertainty to analyze when calculating the rotation curve. These are discussed below:

#### *III.4.1. Systematic Uncertainty in $f_{\text{cutoff}}$*

First of all, the actual determination of $f_{\text{cutoff}}$ is dependent on the nominal selection threshold of $3\sigma$ above the background used. To estimate the uncertainty introduced by our choice of $f_{\text{cutoff}}$, we considered two alternative selections:

- A "loose" selection choosing $f_{\text{cutoff}}$ to be the lowest frequency at $2\sigma$ above the background;
- A "tight" selection choosing $f_{\text{cutoff}}$ to be the lowest frequency at $4\sigma$ above the background.

The uncertainty $\Delta f_{\text{cutoff}}$ was then found by taking the difference between $f_{\text{cutoff}}$ in the nominal and alternative fits. For sharply peaked profiles, this uncertainty was quite small ($\pm 0.01$ MHz). For more broadly peaked profiles, this uncertainty grew as large as $\pm 0.05$ MHz.

#### *III.4.2. Doppler Broadening and Calculating $f_{\text{max redshift}}$*

Another important source of uncertainty arises from Doppler broadening. In particular, if radiation is emitted at frequency $f_0$ from a gas at finite temperature $T$, then the observed radiation obeys a Gaussian distribution:

$$I(f)df \propto \exp\left(-\frac{(f-f_0)^2}{2\sigma^2}\right). \tag{9}$$

Here $I(f)$ is the intensity at frequency $f$. Thus, not every frequency in the profile above corresponds to a genuine emission peak from a galactic source; a frequency could simply be part of the Gaussian fall-off from Doppler broadening.

We estimated the value of $\sigma$ in Eq. 9 by considering radiation from $l = 180°$. We expected this radiation to be sharply peaked at zero redshift, as almost all sources here are moving transverse to the LSR; this was indeed what was observed. Fitting a Gaussian to the peak region of the $l = 180°$ profile, we found $\sigma = 0.046 \pm 0.002$ MHz.

Using the value of $\sigma$ we calculated $f_{\text{max redshift}}$ from $f_{\text{cutoff}}$. In particular, we determined $f_{\text{max redshift}}$ to be the mean emission peak from which we would observe radiation at $f_{\text{cutoff}}$ due to Doppler broadening with width $\sigma$ MHz. We found

$$f_{\text{max redshift}} = f_{\text{cutoff}} + (0.037 \pm 0.028)\ \text{MHz}. \tag{10}$$

Note that the correction to $f_{\text{cutoff}}$ is accompanied by an additional systematic uncertainty.

### III.5. Results and Discussion

Having computed $f_{\text{max redshift}}$, we thus calculated $v(r)$ using Eq. 8 along with the associated systematic uncertainties as computed in Secs III.4.1 and III.4.2. The rotation curve of the galaxy is shown in Fig. 5. We fit the expected $1/\sqrt{r}$ curve from Eq. 7 to the data points $r \geq 4$ kpc. As seen, this is not a good fit to the data; the velocity remains roughly constant at higher radii $r$ instead of falling off. Moreover, using Eq. 6 to find the mass $M(r)$ enclosed within a radius $r$, we find that $M(r)$ continues to increase with radius, even after we expected it to level off after $r \gtrsim 4$ kpc.

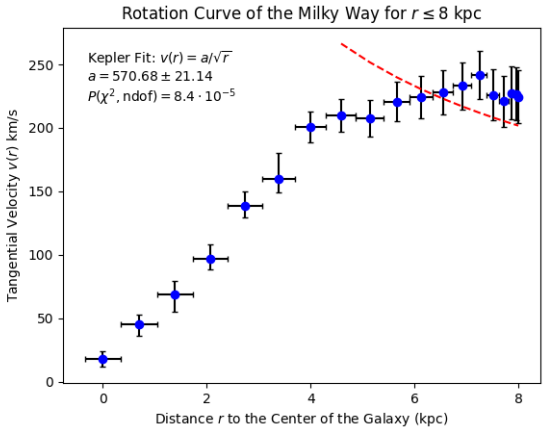


FIG. 5. Rotation curve of the galaxy, along with the expected Keplerian $1/\sqrt{r}$ fit (red line) for $r \geq 4$ kpc. Note that this fit does not describe the data well for this range of $r$.

We thus conclude that there must be a substantial quantity of non-luminous "dark" matter in the region $r \gtrsim 4$ kpc (and indeed outside the galactic bulge $r \gtrsim 1.5$ kpc) not observed directly. This prediction is consistent with previous work [4].


[1] N. Labrum, Australian Journal of Physics **13**, 700 (1960).
[2] M. Shimojo, K. Iwai, A. Asai, S. Nozawa, T. Minamidani, and M. Saito, The Astrophysical Journal **848**, 62 (2017).
[3] L. A. Upton and D. H. Hathaway, Geophysical Research Letters **45**, 8091 (2018).
[4] F. H. Shu, *The physical universe: an introduction to astronomy* (Oxford University Press, 1985).